Available on CMS information server

CMS CR 2007/003

CMS Conference Report

6 February 2007

Heavy Ion Physics with CMS

E.García[a)]

University of Illinois at Chicago, Chicago IL, USA

CMS collaboration

Abstract

The Large Hadron Collider (LHC) will produce heavy ion collisions at the nucleon-nucleon center of mass energy of 5.5 TeV, the highest energy ever available in a controlled environment. This represents an opportunity to study nuclear matter in systems with unprecedented energy densities. Due to the high incident energy, semi-hard and hard processes will be a dominant feature at the LHC. The Compact Muon Solenoid (CMS) heavy-ion program is ideally suited to study the physics of these probes, addressing open questions in the field of Quantum Chromodynamics (QCD). In this paper an overview of the heavy-ion physics capabilities of the CMS detector is presented.

Presented at *VI Latin American Symposium on High Energy Physics*, Puerto Vallarta Mexico, November 1, 2006

Submitted to *AIP*

[a)] email address: ejgarcia@uic.edu

1 Introduction

During the last few years, the four experiments at the Relativistic Heavy Ion Collider (RHIC) have collected a large set of data on nuclear collisions over a wide range of incident energy and system size. There is strong evidence of the formation of a high energy density medium in these collisions, which is strongly interactive, seems thermalized and appears almost opaque to jet-like partons. Furthermore, the data is consistent with the creation of a system with energy densities higher than the critical density expected for the transition to a system where quarks and gluons have achieved asymptotic freedom. A summary of the key observations leading to this description is in Fig. 1: Left panel, normalized charge particle distribution as function of the collision energy for several systems [1]. With the point at 200 GeV, one can estimate that the initial energy density created at τ_0 = 1 cm/c at RHIC is $\sim$ 5 GeV/fm^3, about a factor of ten larger than the energy density of nuclear matter [2]. Center panel, elliptic flow signal v_2 near mid rapidity as a function of the number of participants (centrality) [3]. The large signal of elliptic flow is evidence of early interactions between the produced particles, also the flow signal is close to the value predicted by relativistic hydrodynamics calculation [4], an indication of fast thermalization. Right panel, suppression of the yield on the opposite side on back to back correlation in high p_T charged hadrons [5].

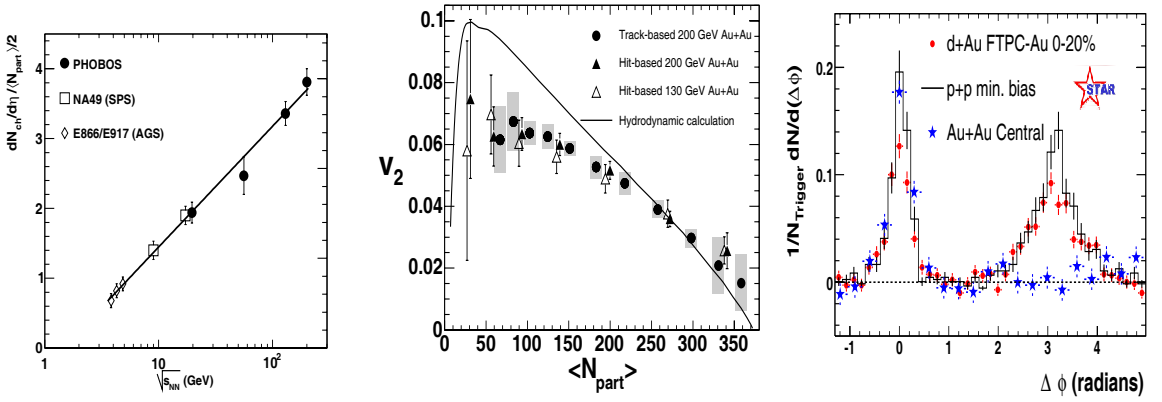

Figure 1: Left panel evolution of the midrapidity charged particle density $dN_{ch}/d\eta|_{|\eta|\leq 1}$, per participating nucleon pair, $N_{part}/2$, as a function of center of mass energy [1], the solid line is a logarithmic extrapolation of the data from lower energies to guide the eye. Center panel elliptic flow of charged particles near mid rapidity as function of centrality in Au+Au collisions [3]. The curve shows the prediction from a relativistic hydrodynamics calculation [4]. Right panel shows azimuthal correlations for p+p, central d+Au and central Au+Au collisions (background subtracted) [5].

At the LHC, the energy densities are predicted to be around 20 times higher than at RHIC, implying a factor of 2 higher for the initial temperature [6]. This is well above the phase transition region between hadronic matter and quark gluon plasma (QGP). Furthermore, at the LHC the higher densities of the produced partons will result in more rapid thermalization, so that the time that the matter will be in a QGP phase is increased by almost a factor of three when compared to RHIC. These conditions may allow the creation of a weakly interacting gas-like QGP state in contrast to the strongly interacting liquid-like state believed to be created at RHIC [7]. In addition to the study of the RHIC base-line measurements, the LHC expands the heavy-ion physics possibilities in the kinematic phase space: larger momentum transfer (Q^2) and lower momentum fraction (x). For example the production of hard probes like high p_T jets, photons, heavy-quark particles (J/ψ) and gauge bosons ($W^{\pm}$, Z^0) will be available at LHC, while many of them are not experimentally accessible at RHIC.

2 Overview of the CMS Detector

CMS offers a high resolution tracking and calorimetry over a uniquely large range in rapidity and 2π-azimuthal coverage. The acceptance of the different elements of the detector is represented in Fig. 2. In addition CMS is complemented with several detector components to characterize particle production at very forward rapidities: CASTOR calorimeter ($5.3 < |\eta| < 6.6$), TOTEM roman pots ($7 < |\eta| < 10$), and the Zero Degree Calorimeter (ZDC) ($|\eta| > 8.3$ for photons and neutrons).

A detailed description of the detector elements is given in the Technical Design Reports [8, 9, 10, 11, 12, 13]. The dominant element of the CMS detector is a superconducting solenoidal coil magnet. It is 13 m long and 6 m in diameter, providing a 4 T field throughout the inner portion of the detector. This inner region holds the highly segmented Si tracker that provides precision tracking of the particle trajectories close to the interaction point. This

information can be used to determine the momentum of the particles going to the more exterior calorimeters and muon detectors. Similar to the tracker the electromagnetic and hadronic calorimeters are arranged in barrels and endcaps located inside the magnet coils. The electromagnetic calorimeter (ECAL) consists of $PbWO_4$ crystals, while the hadronic sampling calorimeters (barrel and endcap) are formed by layers of scintillator and copper. Finally outside the magnet the muon detection system is made of drift tubes, cathode-strip chambers and resistive plate chambers.

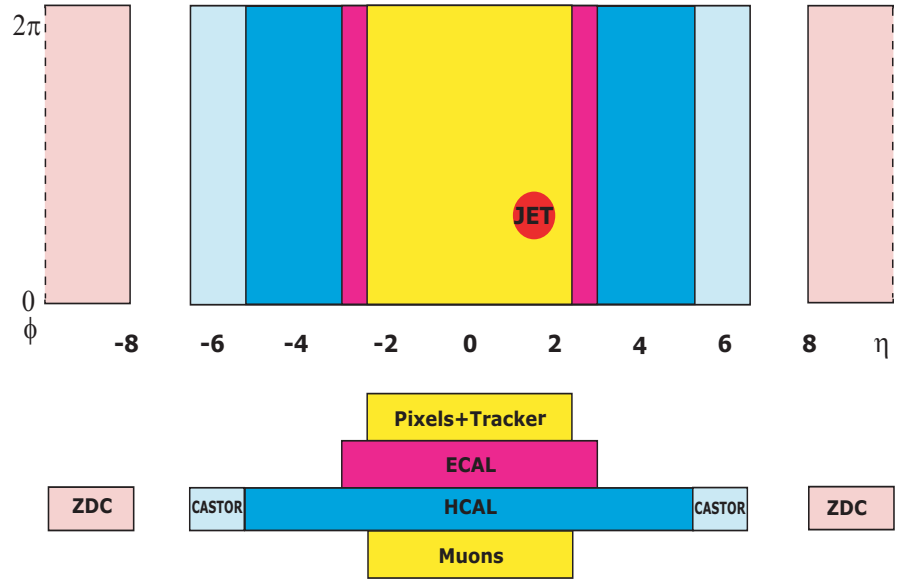

Figure 2: Acceptance of CMS tracking, calorimetry, and muon identification in pseudorapidity and azimuth. The size of a typical jet cone (R = 0.5) is included as an illustration

3 Heavy Ion Physics Capabilities of CMS

The capabilities of the CMS detector provide a unique opportunity to study the new physics potential provided by the heavy ion collisions at the LHC. CMS is designed to deal with p+p collisions at luminosities of $10^{34} cm^{-2} s^{-1}$. At full luminosity there will be, on average, 25 p+p collisions per bunch crossing. In this environment the design resolution and granularity of all detector components have been maximized in order to resolve the high momentum ($p_T > 5$ GeV/c) observables. This makes the detector ideal for the high multiplicity conditions in central heavy ion collisions: the technologies chosen for tracking, calorimetry, and muon identification will allow a read out of CMS with a minimum bias trigger at the full expected 10^{27} cm^{-2} s^{-1}, Pb+Pb luminosity. The CMS and TOTEM detectors will form the largest acceptance system at the LHC. The ZDC and CASTOR will enhance further the acceptance in the forward region, allowing low-x measurements. As for particle identification, the muon system in combination with the silicon tracker will allow studies of the interaction of identified quark jets with the medium. In addition the physics of meson vs. baryon production at large p_T can be studied via the the reconstructed $\pi^0 s$.

3.1 Global Observables

One of the first measurements of CMS from heavy ion collision will be the charged particle multiplicity. The performance of the Si tracker for this measurement was fully simulated for central Pb+Pb collisions for a range of maximum rapidity charged particle yields. The reconstructed charge particle pseudorapidity distribution from simulation is shown in the left panel of Fig. 3, this was calculated using the pixel detector and for $dN_{ch}/d\eta \sim 4000$.

For the study of different physics topics in heavy ions, as heavy quarkonium or hard jet production, it is important to perform measurements at different centralities. Since the forward rapidity region is almost free of final state re-interactions, the transverse energy deposition in the hadron forward calorimeter (HF) or in the ZDC is determined mainly by the initial nuclear geometry of the collision, rather than by final state dynamical effects. These are then the signal that can be better correlated to the impact parameter of the collision. Figure 4 shows the correlation between the transverse energy deposition in HF for 1000 minimum bias Ar+Ar and 1000 Pb+Pb collisions at $\sqrt{s_{NN}}$ = 5.5 TeV (left panel), and the resolution of this measurement (σ_{E_T}/E_T) (right panel) [14]. The resolution is of about 20% up to $\langle E_T \rangle \sim 500$ GeV, for lower values of transverse energy the resolution is degraded due

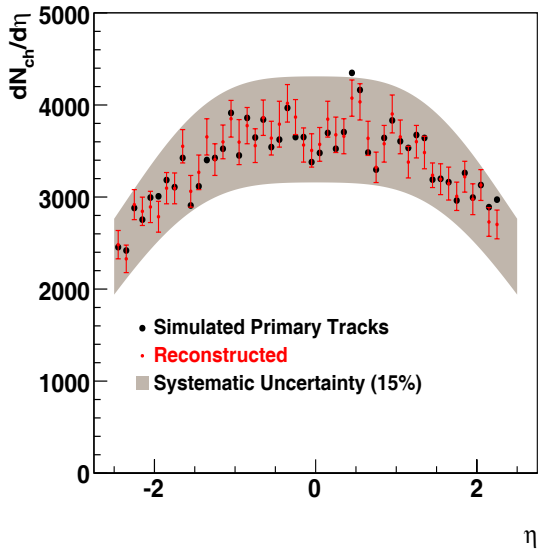

Figure 3: Reconstructed charged particle density $dN_{ch}/d\eta\big|_{|\eta|\leq 1}$ for Pb+Pb collisions at 5.5 TeV. The charge particle density was calculated using the Si tracker with a 2% average occupancy.

to screening of particles produced in the beam pipe. It is expected however that the ZDC response will help to characterize the centrality for more peripheral collisions.

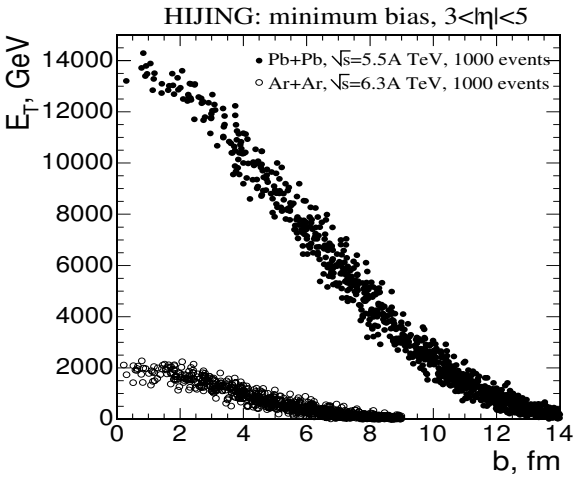

Figure 4: Correlation between transverse energy deposition in HF and impact parameter for minimum bias Ar+Ar and Pb+Pb collisions.

The rescattering and energy loss of hard partons in an azimuthally asymmetric volume can result in an observable azimuthal anisotropy of high-p_T particles and jets. At RHIC studies of the elliptic flow of the azimuthal distributions of produced hadrons relative to their reaction plane have been used to study the question of thermal equilibration at the early stages of the heavy ion collisions. The CMS calorimeters are well suited to measure energy flow and jet azimuthal anisotropy. The ability to reconstruct the event plane and the possibility to observe jet azimuthal anisotropy is shown in Fig. 5 for Pb+Pb collisions at impact parameter $b = 6$ fm. The left panel is the energy deposition in the barrel and end cap regions, and the right panel the difference between the generated and reconstructed azimuthal reaction plane angle. The jet spectra were generated with PYTHIA5.7 and the hydrodynamics input with CMSIM125+ORCA6.2.0 as described in [15].

3.2 Jets and hadron yields

The study at RHIC of the hadron yield and back-to-back hadron correlations above $p_T \geq 3$ GeV/c indicate a pronounced energy loss of fast partons from their interaction with the dense medium created during the collisions. The kinematic region available at the LHC will allow the study of fully reconstructed jets and will extend significantly

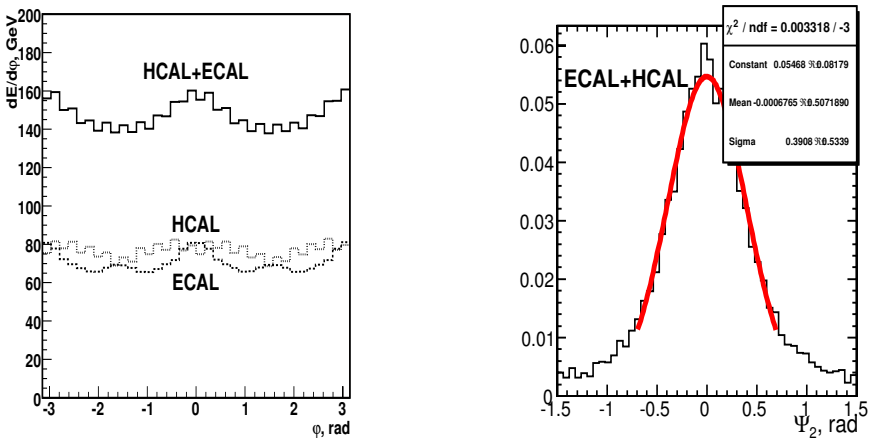

Figure 5: Left panel energy deposition in barrel and endcap regions. ECAL, dashed histogram, HCAL dotted histograms and total deposition (HCAL+ECAL) solid histogram. Right panel is the difference between the generated and reconstructed azimuthal angle Ψ_2 of the reaction plane.

the hadron suppression studies in p_T. For example at the LHC, 10^7 jets with ${E_T}^{jet} > 100$ GeV are produced at $|\eta| \leq 2.6$ for Pb+Pb collisions in one month of running at nominal luminosity. Event jets with $E_T > 50$ GeV can be reconstructed with good efficiency and purity using the calorimeters at CMS. The capabilities for jet reconstruction studies will be enhanced with the Si pixel and tracker detectors that allow the momentum reconstruction of charged hadrons of $p_T > 400$ to 700 MeV/c depending on the multiplicity; with good efficiency, low level of contamination (10% for $p_T \simeq 400$ MeV tracks) and good momentum resolution [16]. Figure 6 shows the tracker reconstruction efficiency (left panel), the jet-finding efficiency and purity for jet reconstruction studies [17] (center), and the nuclear modification factor, R_{AA}, which quantifies the suppression of particle production as function of p_T in simulated Pb+Pb collisions relative to a pp reference (right).

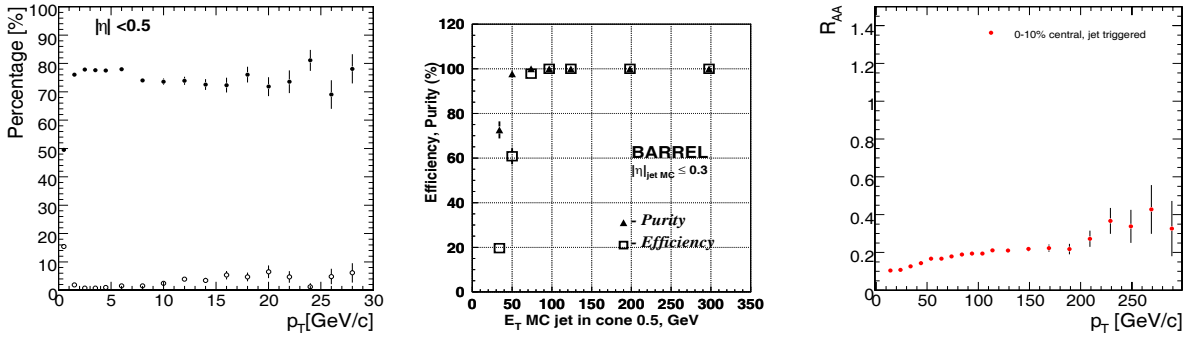

Figure 6: Left panel tracker reconstruction efficiency (full symbols) and fake track rate (open symbols) as a function of the transverse momentum near mid rapidity for central Pb+Pb collisions with $dN_{ch}/d\eta|_{\eta=0} = 3000$, the quality cuts for this figure are optimized for low fake track rate. Center panel is the jet reconstruction efficiency and purity using barrel calorimeters for PYTHIA generated jets in Pb+Pb events with $dN_{ch}/d\eta|_{\eta=0} = 5000$. Right, nuclear modification factor as function of transverse momentum for charged particles for Pb+Pb events triggered on high-E_T jets.

3.3 Quarkonia

One of the proposed signatures of the QCD phase transition is the suppression of the quarkonium production, in particular of the charmonium family (J/ψ,ψ').The charmonium suppression has been observed at CERN SPS and at RHIC but competing mechanisms to color deconfinement (hadronic co-movers interactions and charm quark recombination respectively) have been proposed to explain the observed cross sections. The study of the much heavier bottomonia spectroscopy accessible at LHC is free from the distorting hadronic and coalescence contributions, and can help to clarify this issue. Υ resonances can be detected in the $\mu^+\mu^-$ decay mode with good efficiency (33% for Υ vs. 6% for J/ψ in the CMS detector). Furthermore, studies of the relative yield production of the Υ and Υ' as a function of p_T have been predicted to be highly sensitive to the temperature and size of

the medium created in the collisions addressing information about the dynamics of the high density QCD matter. The feasibility of quarkonia detection shows good resolution efficiency over $|\eta| \leq 2.4$. The expected di-muon invariant reconstructed mass spectra for J/ψ and Υ family after background subtraction are shown in Fig. 7. This reconstruction was studied with a detailed simulation and detector acceptance within central $dN_{ch}/d\eta|_{\eta=0} = 2500$ Pb+Pb collisions [18].

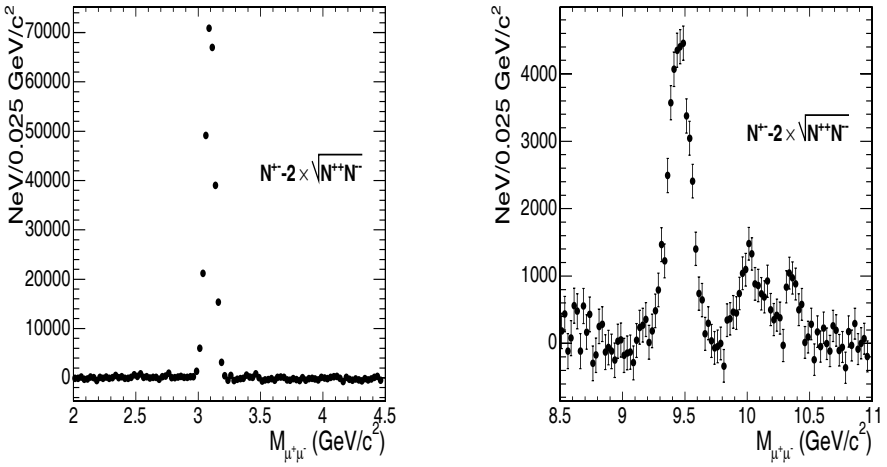

Figure 7: The signal invariant mass distribution, after background subtraction in J/ψ (left) and Υ (right) mass regions. In each case, both muons have $|\eta| < 0.8$.

3.4 Forward Physics

TOTEM and the forward calorimeters CASTOR and the ZDC will enhance the CMS physics program. Parton distribution functions will be mapped out at CMS at low momentum fractions of $x \sim 10^{-6}$ and scales of few GeV^2 of momentum transfer. This coverage will allow the study of the predicted gluon saturation in the framework of the Color Glass Condensate model [19]. For example heavy quark production from ultra-peripheral collisions (UPCs) would be reduced in the presence of CGC relative to the predictions using parton distributions of a free proton. The CMS experiment can measure $\Upsilon \rightarrow e^+e^-$ and $\Upsilon \rightarrow \mu^+\mu^-$ produced in electromagnetic Pb+Pb UPC using the tracker, the ECAL, and the muon chambers tagged with forward neutron detection in the ZDC. Figure 8 shows the expected dimuon invariant mass distributions around the Υ mass predicted by STARLIGHT within the CMS acceptance for integrated Pb+Pb luminosity of 0.5 nb^{-1}. The details of the simulation can be found in [20].

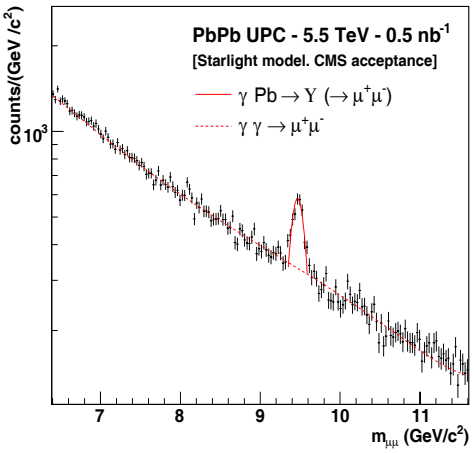

Figure 8: Expected $\mu^+\mu^-$ invariant mass from $\gamma Pb \rightarrow \gamma Pb^* \rightarrow \mu^+\mu^- + Pb^*$ and $\gamma\gamma \rightarrow \mu^+\mu^-$ predicted by STARLIGHT for UPC Pb+Pb collisions at $\sqrt{s_{NN}}$ = 5.5 TeV in the CMS acceptance [20].

4 Acknowledgments

This work was partially supported by the U.S. DOE grant DE-FG02-93ER40802.

References

[1] B. Back *et al.*, *Phys. Rev. Lett.* **88**,22302 (2002).

[2] J.D. Bkorken, *Phys. Rev.* **D** 27, 140 (1983).

[3] B. Back *et al.*, *Phys. Rev.* **C 72**, 031901 (2002).

[4] P. F. Kolb *et al.*, *Phys. Lett.* **B 500**, 232 (2001).

[5] C. Adler *et al.*, *Phys. Rev. Lett.* **90**, 082302 (2003).

[6] I. Vitev and M. Gyulassy, *Phys. Rev. Lett.* **89**, 252301 (2002).

[7] T. D. Lee and M. Gyulassy, nucl-th/0403032 (2004).

[8] CMS HCAL Design Report CERN/LHCC 97-31 (1997).

[9] CMS MUON Design Report CERN/LHCC 97-32 (1997).

[10] CMS ECAL Design Report CERN/LHCC 97-33 (1997).

[11] CMS Tracker Design Report CERN/LHCC 98-6 (1998).

[12] A. Angelis and A. D. Panagiotou, *Jour. Phys.* **G 23**, 18 (1997).

[13] CMS TOTEM Technical Proposal Design CERN/LHC 99-7 (1999).

[14] CMS Note 2001/055 (2001).

[15] CMS Note 2003/019 (2003).

[16] CMS Note 2006/100 (2006).

[17] CMS Note 2006/050 (2006).

[18] CMS Note 2006/089 (2006).

[19] L. McLerran and R. Venugopalan, *Phys. Rev.* **D 49**, 2233 (1994).

[20] David d'Enterria nucl-ex/0610061 (2006).